Study of Solvent Diffusion and Solvent-Induced Crystallization in Syndiotactic Polystyrene Using FT-IR Spectroscopy and Imaging

Andreas Gupper and Sergei G. Kazarian*

Department of Chemical Engineering, Imperial College London, South Kensington Campus, SW7 2AZ London, United Kingdom

Received November 14, 2004

ABSTRACT: Kinetics of solvent diffusion (chloroform) and solvent-induced crystallization in syndiotactic polystyrene (sPS) were investigated by Fourier transform infrared (FT-IR) transmission imaging and single element detector transmission FT-IR spectroscopy. Spatially resolved information from FT-IR imaging experiments under controlled environmental conditions (temperature and solvent vapor pressure) and with uniaxial solvent diffusion into the polymer was used to monitor the appearance of δ crystalline sPS as a function of solvent exposure time. From a series of time-resolved FT-IR images polymer crystallization kinetics at various positions in the polymer and solvent diffusion coefficients were determined. The imaging experiments proved that solvent diffusion is the limiting factor in the overall crystallization process of a sPS sample. FT-IR images revealed that the full extent of crystallinity is reached before the equilibrium concentration of the solvent in the semicrystalline polymer is established at any location in the sample. Single element detector transmission FT-IR measurements indicated that the kinetics of the crystallization process strongly depends on solvent vapor pressure. A critical value of solvent concentration in the polymer needs to be achieved in order to observe any polymer crystallization. This critical value and the crystallization kinetics in a solvent saturated atmosphere were also revealed.

Introduction

Solvent-induced crystallization in polymers is fundamental for processing and applications of polymeric materials. Production and use of many commercially important polymers benefit from a deeper understanding of the dynamic processes, such as morphological changes and crystallization, in polymer/solvent systems.

Vibrational spectroscopy is a well-established method to study conformational changes in polymers. Recently, with the development of global Raman imaging and Fourier transform infrared (FT-IR) imaging instruments, it became possible to obtain the spatial distribution of components in composite materials or the distribution of different morphologies in a polymer. It is now also feasible to study dynamic processes on the time scale of the image acquisition process by observing larger sample areas with high spatial resolution. These improvements together with more efficient detectors and better instrumentation in general considerably increased the number of vibrational spectroscopic applications in polymer science. In this paper we introduce a new application, namely spatially resolved in situ investigations on the kinetics of solvent-induced polymer crystallization by FT-IR transmission imaging and single element detector transmission FT-IR spectroscopy. The paper also extends the recently presented application of FT-IR imaging for studies of mass transport in polymer/solvent systems to determine solvent diffusion coefficients.

The polymer under investigation was syndiotactic polystyrene (sPS). The existing applications and the great potential for further development of smart technologies are the reasons for a high academic as well as industrial interest. Many studies have focused on solvent diffusion and the kinetics of phase transformations, an especially important feature of the material.

Polystyrene with high yields of syndiotactic conformation was synthesized for the first time in the early 1980s. In contrast to the atactic and isotactic forms it has the tendency to crystallize very quickly and to a relatively high extent on exposure to temperatures above T_g or on exposure to certain solvents. This behavior adds to the favorable properties of high melting temperature and chemical resistance of sPS, which were already found for the other modifications, by improving the mechanical properties of the material. In the course of its structural characterization by many different techniques, it was found that sPS can appear in more than one crystalline form and that it shows a complex polymorphic behavior. Today we know of four main crystalline modifications and several subforms. A principal distinction can be made between the transplanar or TTTT all-trans α and β forms with all the phenyl side groups trans to each other and the helical or TTGG γ and δ forms, where macromolecules arrange in a helical conformation and the phenyl side groups are trans−trans−gauche−gauche to each other along the polymer backbone. The first two modifications are obtained by heat treatments above the glass transition temperature or cooling from the melt where the β form is the thermodynamically most stable of all of them. To get sPS in its helical conformation, a step involving solvents, i.e., casting from solution, precipitation from solution, or exposure of an amorphous sample to a suitable solvent, is required. The difference between γ and δ forms is based on the fact that in the δ modification solvent molecules form a complex with the single helical chains. This is not the case in the γ form where the single chains are consequently packed closer to each other and at a higher density. The amorphous form with randomly oriented macromolecular chains, which is the raw material for the investigations presented in this paper, is obtained from quenching the material from the melt. A definition of the different morphologies and their

* Corresponding author. E-mail: s.kazarian@imperial.ac.uk.

10.1021/ma0476590 CCC: $30.25
Published on Web 02/17/2005

nomenclature was published by Guerra et al.[1] in 1990 and will be used throughout this text. An overview of phase transformations is summarized in a paper by Keller et al.[2] An important subform of sPS that is of particular interest for membrane applications is the so-called mesophase. It is characterized by the helical arrangement of the macromolecular chains and cavities between them as in the δ modification. However, in the mesophase these cavities are not occupied by solvent molecules that were used to introduce crystallinity but are free to trap new molecules which are of appropriate size and shape to fit into these empty spaces. Normally it is produced via the δ modification[3,4] whose crystallization kinetics is studied in this paper.

The use of solvents and their effects on amorphous sPS were studied by Immirzi et al.[5] It was soon recognized that some organic solvents introduce the γ and some the δ form. The forms can be distinguished by wide-angle X-ray spectroscopy[1] or vibrational spectroscopic techniques.[6−8] Vibrational spectroscopy is well-suited and widely used to investigate sPS. Based on normal-coordinate analysis,[9] the effects of inter- and intrachain interactions in different molecules on vibrational spectra were elucidated, and bands could be assigned to be indicative of specific sPS modifications.[6] With this well-established background and all required band assignments known, the new possibilities of FT-IR imaging[10−12] could be employed in polymer science to derive spatially resolved information on dynamic polymer processes in-situ.

Experimental Section

Samples. A film of amorphous s-PS has been supplied by Dr. Y. P. Handa. For all experiments the dimensions of the sample were about 1 mm × 1 mm × 50 μm. For solvent vapor generation liquid chloroform of 99.0% purity and liquid toluene of 99.5% purity, supplied from BDH Laboratory Supplies, UK, were used as delivered.

Equipment. FT-IR transmission spectra were acquired with an IFS 66S spectrometer coupled to an IRscope II infrared microscope (Bruker Optics). Single element detector spectra were recorded with a conventional mercury cadmium telluride (MCT) detector and FT-IR images with a 64 × 64 focal plane array (FPA) detector consisting of 4096 single MCT detector elements. The image area corresponds to 266 × 266 μm^2. The spectral resolution is 2 cm^{-1} in all single element detector spectra and 8 cm^{-1} in spectra used to build up FT-IR images. In spectra for image generation the lower spectral resolution and a limited wavenumber range, 1800−900 cm^{-1} compared to 4000−600 cm^{-1}, was chosen to reduce the acquisition time required to obtain spectra for one FT-IR image (about 52 s to acquire one image). All experiments were carried out under controlled environmental conditions (relative solvent vapor pressure and temperature) in a VGI 2000M cell (surface measurement systems).[13,14] Different solvent vapor pressures in the atmosphere surrounding the sample are achieved by mixing a flow of dry air with a flow of solvent saturated air. Solvent vapor concentrations are reported accordingly as the percentage of solvent saturated air in the mixed gas flow entering the sample chamber. This is the way solvent vapor concentrations are controlled in the VGI equipment.

Experimental Details. To obtain spatially resolved information about solvent diffusion and polymer crystallization in the region near the polymer/solvent interface, a special experimental setup is needed. The arrangement described in a previous paper[15] fulfils the requirements of limiting solvent diffusion to a uniaxial process and of allowing in-situ transmission FT-IR image acquisition where the probing infrared beam is perpendicular to the direction of solvent diffusion. The feasibility of the approach and FT-IR images of evolving δ crystalline areas in s-PS after different exposure times to toluene vapor have been reported in the earlier paper. For the investigations presented here, the CaF_2 windows have been replaced by a set of BaF_2 windows (see Figure 1 in ref 15). With this improvement the accessible infrared information has been extended down to 900 cm^{-1}, which is the detection limit of the FPA detector. In the previous setup the CaF_2 windows drastically reduced the amount of transmitted infrared light intensity below 1100 cm^{-1} and prevented any meaningful signal detection below 1000 cm^{-1}.

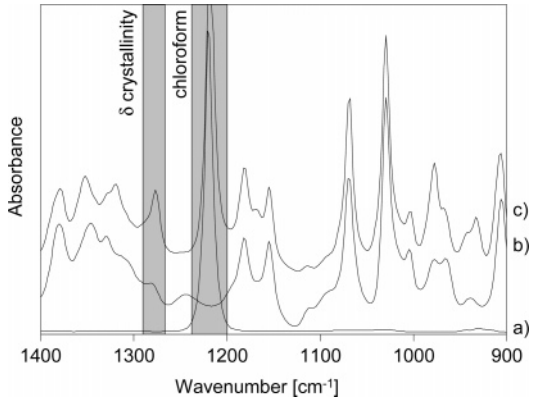

Figure 1. Reference FT-IR spectra of chloroform (a), amorphous (b), and δ crystalline (c) syndiotactic polystyrene. The band at 1220 cm^{-1} corresponds to the bending mode of chloroform. This band has been used to determine the type of solvent diffusion behavior and the solvent diffusion coefficient. The band of sPS at 1275 cm^{-1} was used to follow the crystallization process of the polymer.

To study polymer crystallization kinetics as a function of solvent vapor pressure by using a single element detector, a simpler experiment setup was used. A sPS film was placed on a BaF_2 window within the controlled environment cell, which was sealed against the outer atmosphere by two thin BaF_2 windows. The solvent vapor flow was not restricted to any particular direction on entering the polymer film. As the film was not pressed between two windows, diffusion into the film from the bottom and top side was also possible. Spectral changes indicating the phase transformation from amorphous to δ crystalline sPS were monitored with a time resolution better than 5 s. The percentage of solvent saturated vapor in the cell was varied between 50 and 99% of its maximum value.

Results and Discussion

Chloroform Diffusion. Figure 1 shows reference FT-IR spectra (measured with 4 cm^{-1} spectral resolution) of the solvent (chloroform, spectrum a) as well as amorphous (spectrum b) and δ crystalline sPS (spectrum c). The latter sample was prepared by inducing crystallinity with chloroform. The band at 1220 cm^{-1} does not belong to a vibrational mode of the polymer but arises from a vibrational mode of chloroform molecules which formed a complex with the helical conformation of the polymer chains and chloroform dissolved in the amorphous domains of the polymer. All spectra are shown in the region from 1400 to 900 cm^{-1}, which is accessible in imaging and single element detector experiments and contains information on solvent uptake as well as phase transformations of sPS. Two gray bars in Figure 1 mark the integrated wavenumber regions indicative of δ crystallinity and chloroform.

The integrated absorbance of the chloroform bending mode, δ(H−C−Cl), at 1220 cm^{-1} was used to study the distribution of solvent in sPS as a function of time. When the integrated band absorbance value is plotted vs the horizontal pixel number of the FPA detector, plots

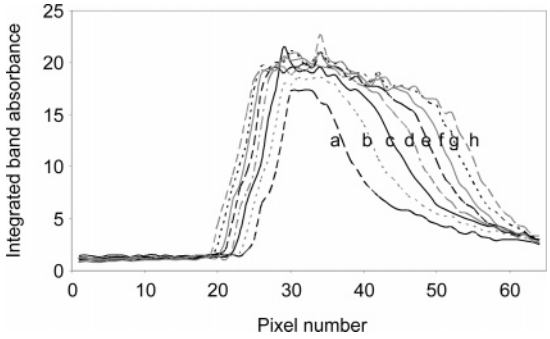

Figure 2. Position of the front of chloroform as a function of horizontal pixel number of FPA; the gas phase is on the left side, and the polymer is on the right side. Profiles are based on the values of the integrated absorbance of the band of chloroform at 1220 cm^{-1}. The sample was exposed to vapor of chloroform for 52 s in profile a. For profiles b−h solvent exposure time increases in steps of 52 s. Ten vertical detector elements have been co-added for an enhanced signal-to-noise ratio.

with spatially resolved information become available that demonstrate how the solvent front progresses toward the bulk of the film. In Figure 2, several concentration profiles across the film (measured as a function of the horizontal pixel number of the FPA detector) are shown for different solvent exposure times. In this figure the gaseous chloroform was supplied from the left side. The absorbance of solvent vapor is very low compared to the signal from the condensed solvent within the polymer. From these plots it can be recognized that with longer solvent exposure time the solvent front moves to the right and further into the polymer. Profile a shows the solvent distribution in the polymer after 52 s exposure time. Profiles b−h were registered afterward in 52 s intervals. To obtain a better signal-to-noise ratio, the responses of 10 vertical rows of detector elements have been coadded. This approach is only feasible without introducing an error in diffusion distances if the diffusion process is parallel to the horizontal lines of the FPA detector elements. For the presented plots this was true to a very good approximation due to an appropriate arrangement of the sample under the microscope. From the solvent concentration profiles, and recognizable by the shift of the polymer/solvent interface to the left after increasing exposure time, it can be seen that the polymer film swells on interaction with the solvent. Furthermore, Figure 2 verifies the fact that by using solvent in its gaseous state no polymer dissolution is observed even at longer exposure times because there is a sharp interface between the polymer and the gaseous solvent supply at any time. Figure 2 also reveals the equilibrium concentration of chloroform within the polymer by the plateau of the concentration value around 20, which remains almost constant from the polymer/solvent interface to the solvent diffusion front. Although it is not possible from this number to deduce the number of solvent molecules required to plasticize a polymer chain, it suggests that there is equilibrium between the condensed solvent phase within in the polymer and the gaseous supply.

To obtain quantitative information on the diffusion of chloroform, the polymer film edge and the position of the chloroform diffusion front after different solvent exposure times were determined from the plots derived from FT-IR images. The polymer film edge was found by integration of the in-plane bending modes of sPS at

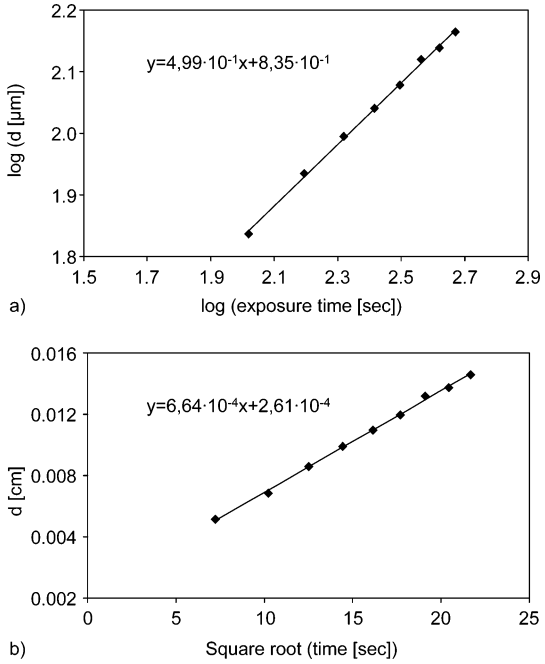

Figure 3. (a) A log−log plot of chloroform diffusion front distance (d in μm) from the polymer/solvent interface vs solvent exposure time provides the diffusion exponent α. Here $\alpha \approx 0.5$ suggests Fickian diffusion behavior for chloroform in sPS. (b) The diffusion front distance from the polymer/solvent interface (d in cm) is plotted vs the square root of solvent exposure time. From the slope of the linear regression the solvent diffusion coefficient D at 20 °C was calculated to be 4×10^{-7} cm^2 s^{-1}.

1420 and 1530 cm^{-1} that have strong absorbances The film edge was defined as the point at 50% of the maximal integrated absorbance value. In a similar manner the position of the solvent front was found by integrating the 1220 cm^{-1} band of chloroform and using the 50% value of the maximum absorbance. The type of solvent diffusion can then be determined by the so-called diffusion exponent α. According to ref 16, where this procedure has been successfully applied, an α value of 0.5 indicates Fickian and a value of 1.0 case II type diffusion behavior. By plotting the logarithm of the solvent diffusion front distance (d in μm) vs the logarithm of solvent exposure time, as shown in Figure 3a, α is directly accessible as the slope of a linear fit to the data points. All experiments with chloroform gave α values of about 0.5 and indicate Fickian diffusion behavior. Figure 3b shows how the solvent diffusion coefficient (D) of chloroform was obtained from a plot of the solvent diffusion front distance (d in cm) vs the square root of solvent exposure time. A linear fit of the data points of the slope of this curve represents the square root of D. The experimentally derived diffusion coefficient of chloroform in sPS at 20 °C is 4×10^{-7} cm^2 s^{-1}. This value is in excellent agreement with the diffusion coefficient of liquid chloroform from mass uptake experiments by Vittoria et al.[17] Chloroform shows the same type of diffusion as toluene but diffuses faster compared to toluene ($D = 7 \times 10^{-8}$ cm^2 s^{-1}) at 20 °C.[15] Considering the smaller size of chloroform molecules, these results confirm the general expectations, but here solvent diffusion was directly determined from spatially resolved FT-IR images, where a uniaxial diffusion process was monitored online. Tashiro and coworkers compared this diffusion behavior from measurements through the whole thickness of the film.[18,19]

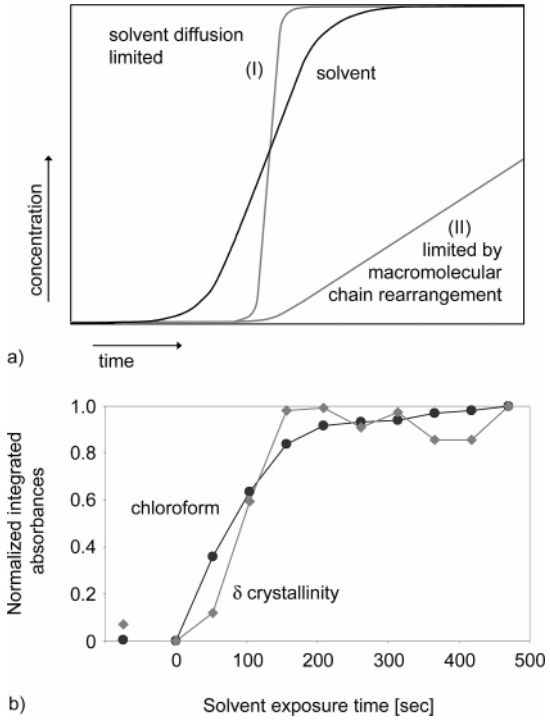

Figure 4. (a) Limiting situations for the overall crystallization process of a sPS sample: (I) the rate of solvent diffusion into the polymer limits the crystallization progress; (II) rearrangement of macromolecular chains is slow compared to the movement of the solvent diffusion front. (b) Experimentally observed increase in degree of crystallinity (squares) and solvent (circles) concentration 50 μm away from the polymer/solvent interface vs solvent exposure time (FPA pixel row 41).

It is rather remarkable that the diffusion coefficient of chloroform when supplied in its gaseous form is about the same as with a supply of liquid chloroform.[17] This indicates that an increase in the amount of solvent present does not affect the plasticization of the polymer and solvent diffusion compared to that of a saturated chloroform atmosphere.

Crystallization Kinetics of sPS. Solvent-induced crystallization of sPS has been studied in this work beside the phenomenon of solvent diffusion. In the amorphous state the randomly oriented polymer chains rearrange to a helical conformation when they are exposed to suitable solvents. It has been shown by Vittoria et al.[17] that chloroform induces a helical crystalline form of sPS (δ form with solvent molecules form a complex with the helical macromolecular chains). Thermodynamics of the solvent-induced crystallization has recently been reviewed.[20]

The fundamental question addressed here is whether the overall crystallization process in a sPS sample is limited by the macromolecular chain rearrangements or by the solvent diffusion into the polymer. Solvent diffusion is a prerequisite for the crystallization process. It is needed to plasticize the amorphous polymer in order for the macromolecular chains to be able to rearrange. Figure 4a shows schematically the (normalized) concentration/time profiles for the two limiting situations. The black solid line represents the solvent concentration profile at a certain position in the polymer and applies for both cases discussed below. It shows that with time solvent diffuses into the sample, reaches the selected position, concentration of the solvent increases to the equilibrium level, and remains constant thereafter. The gray lines illustrate the amount of δ crystalline sPS at the same specific location in the sample for two possible scenarios. Curve I indicates that there must be a certain amount of solvent before the macromolecules start to rearrange. As soon as this critical value of solvent concentration is reached, the reorganization into the thermodynamically more stable δ crystalline modification begins. This happens so quickly that the polymer is already crystallized to its maximum extent when the solvent has not yet reached its overall equilibrium concentration. The continuing increase in the overall amount of solvent occurs to the amorphous domains of sPS. In this case it can be assumed that for the crystallization of an entire sPS sample the rate of solvent diffusion through the semicrystalline polymer is the limiting factor. Curve II represents the situation where the rearrangement of the macromolecular chains from the randomly coiled amorphous state into the helical conformation is the rate-determining step in the crystallization process. The figure shows that no rearrangements take place here before a certain amount of solvent is present, as in the previous case. However, even when this lower critical value is surpassed, reaching the maximum possible formation of δ crystalline domains occurs slowly. Curve II shows that it takes much longer for the polymer to crystallize than for the solvent to reach its maximum or equilibrium level. In Figure 4b, the normalized absorbance for the spectral bands of chloroform and δ crystallinity at a distance of 50 μm away from the polymer/solvent interface (FPA pixel row 41) in the polymer are shown vs solvent exposure time. It is easy to recognize that the pattern reflects curve I in Figure 4a and suggests a diffusion-limited crystallization process. The two data points for each curve at time less than zero (that are not interconnected with the rest of the curves) were acquired before the time when the solvent flow was switched on. A slight decrease in crystallinity at the beginning is possibly due to the plasticization of the polymer. The randomly occurring TTGG segments in the amorphous phase can change conformations easier before they start the crystallization process. Concentration profiles of solvent and the degree of crystallinity at different points in the polymer, obtained from FT-IR imaging data, can also answer the above question. Figure 5 shows the normalized integrated absorbance for the corresponding spectral bands of both parameters (solvent and δ crystallinity) across the film (as a function of the horizontal pixel number of the FPA detector) after two solvent exposure times, 52 and 416 s, respectively. The solid

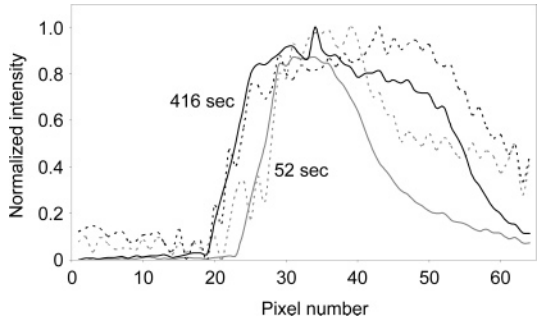

Figure 5. Normalized integrated absorbance profiles for the spectral bands of chloroform and δ crystallinity as a function of the horizontal pixel number of the FPA detector. The solid lines represent solvent and the dashed lines crystallinity profiles. Gray lines correspond to a solvent exposure time of 52 s whereas the black lines belong to profiles obtained after 416 s of exposure to chloroform.

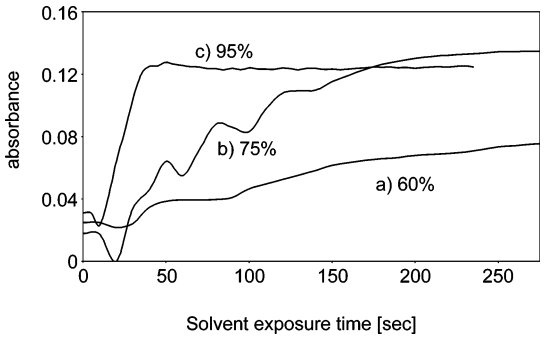

Figure 6. Absorbance of the band at 1275 cm^{-1} band, an indicator of δ crystallinity, is plotted vs chloroform vapor exposure time. Chloroform concentrations were set to levels of 60% (a), 75% (b), and 95% (c) solvent-saturated air entering the sample compartment as indicated in the figure. All experiments were carried out at 20 °C.

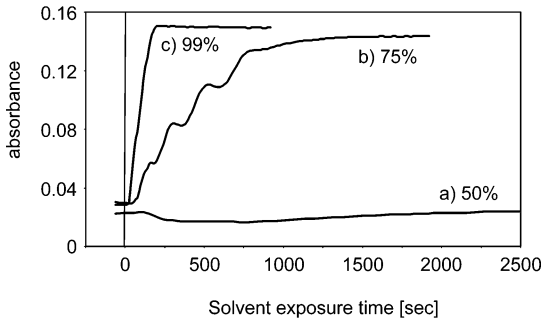

Figure 7. Absorbance of the band at 1275 cm^{-1}, which is an indicator of δ crystallinity, as a function of toluene vapor exposure time. The toluene vapor was set to 50% (a), 75% (b), and 99% (c) of solvent-saturated gas entering the sample compartment. All experiments were carried out at 20 °C.

lines represent concentration profiles of chloroform whereas the dashed lines belong to the integrated absorbance value of the 1275 cm^{-1} band, an indicator of δ crystallinity. The crystallinity profiles appear noisier because the 1275 cm^{-1} band is considerably weaker than the strong chloroform absorption band, and because of the short image acquisition times, no better signal-to-noise ratio was achieved for the crystallinity band. Nevertheless, it can be clearly recognized from the profiles at both solvent exposure times that the crystallization process is completed before the solvent equilibrium is achieved in the semicrystalline polymer. From this observation it can be deduced that the overall crystallization process is limited by the solvent diffusivity and plasticization of the polymer rather than by the rearrangement of macromolecular chains.

Next, the following questions have been addressed: How fast is the actual crystallization process occurring, and what is the lower critical solvent concentration to introduce crystallinity?

These questions about the kinetics of polymer crystallization were investigated by FT-IR spectra acquired with a single element detector at constant temperature and as a function of solvent vapor pressure. Polymer films were exposed to different solvent vapor concentrations and were measured in transmission mode in constant time intervals. The absorbance of the 1275 cm^{-1} band, which is assigned to a TTGG backbone vibration in the helical δ crystalline modification of sPS, was used to follow the crystallization process occurring as a response to solvent vapor exposure. Depending on the relative amount of solvent in the atmosphere drastic changes in terms of crystallization kinetics were observed. In Figure 6, the absorbance of the 1275 cm^{-1} band is plotted against solvent exposure time. Curves a−c correspond to polymer films that were subjected to chloroform levels of 60, 75, and 95% of the saturated solvent vapor. The temperature was held constant at 20 °C in all experiments. At the highest solvent vapor concentration the overall crystallization process is finished in about 60 s. As soon as the solvent vapor pressure is lowered, the crystallization process takes much longer as visible from the other curves presented in Figure 6. When the percentage of saturated chloroform vapor in the sample chamber gets to 50%, it takes more than 4 h for the crystallization process to complete. At solvent pressures below this value band changes indicating the plasticization process and a lowering the content of TTGG formation in the semicrystalline polymer was observed, but no band increase was observed. This again is a proof that solvent molecules plasticize the material to make the polymer chains more mobile before the actual crystallization can begin. The solvent molecules move in between single macromolecular chains, increase the distance between them, and allow the polymer to rearrange. The higher the amount of solvent present, the easier it is for the macromolecules to rearrange. It is easiest for them to move in solutions, but then intramolecular interactions are smaller and more energy is gained from the solvation process rather than by adopting a compact crystalline form. When the solvent concentration is reduced, the equilibrium shifts to the other side. On exposure of the samples to solvent vapors the available amount of solvent is drastically reduced compared to solutions, and it becomes much more difficult for the macromolecular chains to rearrange. Therefore, the time it takes to obtain a crystalline sample is expected to rise with every further reduction in solvent concentration. This behavior was observed experimentally and is reflected in Figure 6. At a certain point the amount of solvent becomes too small to allow chain ordering. There is still some solvent present in the polymer but not enough for a whole macromolecular chain to move and get into the thermodynamically favorable position. The long chains can be considered as being frozen under the glass transition temperature or equally the amount of solvent is not high enough to reduce the glass transition temperature below the temperature of the experiment. This concept also confirms the expected and measured result (not shown in a separate figure) that by rising the temperature the same amount of solvent introduces crystallinity at a higher rate.

Similar experiments were carried out to study the crystallization kinetics of sPS on exposure to toluene. Figure 7 reviews the amount of crystallinity at exposure levels of 50, 75, and 99% saturated solvent gas in the total gas flow entering the sample compartment and confirms the conclusions drawn for chloroform. It takes about 200 s to complete the crystallization process in a toluene-saturated gas atmosphere at 20 °C. With a reduction of solvent vapor concentration to 75% of solvent saturated gas in the total gas flow crystallinity is reached after about 1500 s. If the percentage of solvent saturated gas in the overall gas flow is reduced to 60% (not shown in Figure 7), it is still possible to observe an increase in crystallinity on a reasonable time scale. Experiments were stopped after 4 h although at this time equilibrium in the system has not been reached yet. Finally, when the percentage of solvent-

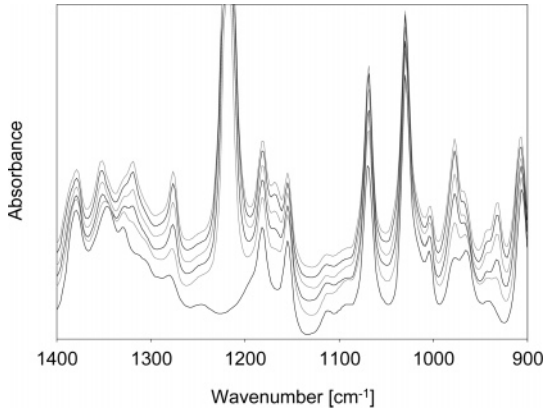

Figure 8. FT-IR spectra of sPS after different exposure times to 60% chloroform saturated gas (and 40% dry air) entering the sample compartment. Exposure times increase from the bottom spectrum, which shows amorphous sPS at the beginning of the experiment, to the top spectrum, which represents crystalline sPS after 30 min solvent exposure. Spectra 2−4 (from bottom to top) correspond to 150, 300, and 450 s solvent exposure time.

saturated vapor in the air flow is reduced to 50%, a decrease in intensity of the crystallinity peak can be recognized very clearly (visible also in all other profiles). It appears that crystallinity decreases before it rises again, but this effect is probably due to the plasticization of the polymer and changes of the band shape that may affect the baseline and hence the absorbance values. Kaji and co-workers[21] described band changes as a result of solvent−polymer interaction, but their studies concentrated mostly on the wavenumber region below 600 cm^{-1} which was not accessible for the FPA detector used in these investigations. Figure 1 also shows several spectral changes occurring close to the band at 1275 cm^{-1} on induction of crystallinity that may cause changes of the baseline and be responsible for this kind of fluctuation which is also visible at higher solvent pressures.

In the described experiments the appearance and growing behavior of several bands in the spectrum were closely followed. Figure 8 shows single point FT-IR transmission spectra after different exposure times to a chloroform vapor (60% solvent saturated gas in the total gas stream). In contrast to observations made by Tashiro et al.,[18,19] we did not find a significant delay in the appearance of bands but found just an overall reduction in their growing rate. Therefore, the concept of critical sequence lengths which has been provided as an explanation for their observations must still be considered in more detail.

Conclusions

We have applied in-situ FT-IR spectroscopy and imaging to study mass transport and phase transformations in syndiotactic polystyrene. Simultaneous observation of these processes was possible with sufficient time and spatial resolution in transmission FT-IR spectroscopic imaging experiments. The diffusion coefficient of chloroform was determined from a Fickian fit of the position of the diffusion front as a function of time. The diffusion coefficient of chloroform at 20 °C in sPS was calculated to be $D = 4 \times 10^{-7}$ cm^2 s^{-1}. This value was compared with the corresponding value for diffusion of toluene. Furthermore, this work provided information on the rate of phase transformation from amorphous to helical, δ crystalline form of sPS, as a function of a partial solvent vapor pressure. By varying the amount of solvent in the atmosphere surrounding the sample, it was possible to find the lower critical solvent vapor pressure that is required to initiate the crystallization process. The presented in-situ FTIR imaging approach is not limited to sPS and can be applied to diffusion and crystallization studies of a wide range of polymers.

Acknowledgment. The authors thank Y. P. Handa for providing the sPS sample, Dr. K. L. A. Chan for his help and advice, the FWF−Austrian Science Funds for granting an Erwin Schrödinger visiting fellowship (project J2287-B10) to Andreas Gupper, and EPSRC (GR/S57600/01) for financial support.

References and Notes

(1) Guerra, G.; Vitagliano, V. M.; De Rosa, C.; Petraccone, V.; Corradini, P. *Macromolecules* **1990**, *23*, 1539−1544.
(2) Kellar, E. J. C.; Galiotis, C.; Andrews, E. H. *Macromolecules* **1996**, *29*, 3515−3520.
(3) Reverchon, E.; Guerra, G.; Venditto, V. *J. Appl. Polym. Sci.* **1999**, *74*, 2077−2082.
(4) Rani, D. A.; Yamamoto, Y.; Mohri, S.; Sivakumar, M.; Tsuijta, Y.; Yoshimizu, H. *J. Polym. Sci., Part B: Polym. Phys.* **2003**, *41*, 269−273.
(5) Immrizi, A.; De Candia, F.; Iannelli, P.; Zambelli, A.; Vittoria, V. *Makromol. Chem., Rapid Commun.* **1988**, *9*, 761−764.
(6) Moyses, S.; Spells, S. J. *Macromolecules* **1999**, *32*, 2684−2689.
(7) Musto, P.; Tavone, S.; Guerra, G.; de Rosa, C. *J. Polym. Sci., Part B: Polym. Phys.* **1997**, *35*, 1055−1066.
(8) Musto, P.; Mensitieri, G.; Cotugno, S.; Guerra, G.; Venditto, V. *Macromolecules* **2002**, *35*, 2296−2304.
(9) Reynolds, N. M.; Hsu, S. L. *Macromolecules* **1990**, *23*, 3463−3472.
(10) Koenig, J. *Adv. Mater.* **2002**, *14*, 457−460.
(11) Ribar, T.; Bhargava, R.; Koenig, J. L. *Macromolecules* **2000**, *33*, 8842−8849.
(12) Kazarian, S. G.; Chan, K. L. A. *Macromolecules* **2003**, *36*, 9866−9872.
(13) Jervis, H.; Kazarian, S. G.; Chan, K. L. A.; Bruce, D.; King, N. *Vib. Spectrosc.* **2004**, *35*, 225−231.
(14) Chan, K. L. A.; Kazarian, S. G. *Vib. Spectrosc.* **2004**, *35*, 45−49.
(15) Gupper, A.; Chan, K. L. A.; Kazarian, S. G. *Macromolecules* **2004**, *37*, 6498−6503.
(16) Snively, C. M.; Koenig, J. L. *J. Polym. Sci., Part B: Polym. Phys.* **1999**, *37*, 2261−2268.
(17) Vittoria, V.; de Candia, F.; Iannelli, P.; Immirzi, A. *Makromol. Chem., Rapid Commun.* **1988**, *9*, 765−769.
(18) Tashiro, K.; Ueno, Y.; Yoshioka, A.; Kobayashi, M. *Macromolecules* **2001**, *34*, 310−315.
(19) Tashiro, K.; Yoshioka, A. *Macromolecules* **2002**, *35*, 410−414.
(20) Ray, B.; Elhasri, S.; Thierry, A.; Marie, P.; Guenet, J.-M. *Macromolecules* **2002**, *35*, 9730−9736.
(21) Matsuba, G.; Kaji, K.; Nishida, K.; Kanaya, T.; Imai, M. *Macromolecules* **1999**, *32*, 8932−8937.

MA0476590